Characterization of the N-Terminal Targeting Signal Binding Domain of the Mitochondrial Outer Membrane Receptor, Tom20[†]

Enrico Schleiff*,[‡] and Joanne L. Turnbull*,[§]

Department of Biochemistry, McIntyre Medical Science Building, McGill University, Montreal, Canada H3G 1Y6, and Department of Chemistry & Biochemistry, Concordia University, Montreal, Canada H3G 1M8

Received April 2, 1998; Revised Manuscript Received July 14, 1998

ABSTRACT: hTom20 is an outer mitochondrial membrane receptor involved in protein translocation. The cytosolic domain (aa30−145) and selected truncated versions of this domain were overexpressed and purified to study the structure−function relationship of this protein. Our studies reveal that the secondary structure of the cytosolic domain is very resistant to unfolding by guanidine−HCl and urea and is stabilized mainly by hydrophobic interactions. However, the tertiary structure of the N-terminal targeting signal binding domain (aa30−90) is more flexible. The first 30 amino acids of the cytosolic domain (aa30−60) are involved in recognizing N-terminal targeting signals and in stabilizing the cytosolic domain on the lipid surface. Moreover, we show that specifically aa30−48 interact with the membrane surface; a construct containing aa48−145 will only bind to the membrane surface in the presence of an N-terminal targeting signal peptide. The C-terminal region of hTom20 (aa141−145) interacts with the N-terminal region of hTom20, helping to stabilize the proper conformation of the N-terminal targeting signal binding domain. Finally, hTom20 interacts with the N-terminal targeting signal of preornithine carbamyl transferase fused to dihydrofolate reductase very weakly ($K_d = 8\ \mu M$), as would be expected if this interaction was the first in a series orchestrated by the import receptor complex to draw the targeted protein into the mitochondrion.

Tom20[1] is a major receptor of the mitochondrial translocation complex (*1*) and its general function was investigated in detail both in vivo and in vitro (*2*−*6*). Tom20 recognizes proteins containing N-terminal targeting signals as well as proteins containing internal targeting signals (*7*, *8*).

A deeper understanding of the protein recognition process can be gained from investigating the structure−function relationship of the components of the import complex. In the present report we describe the structural and functional behavior of the N-terminal portion of the cytosolic domain (aa30−90). The secondary structure of the intact cytosolic domain is stabilized by mainly hydrophobic interactions and is very resistant to unfolding by denaturants. On the other hand, the tertiary structure of hTom20 is flexible in the region aa30−60. The C-terminal domain (aa141−145) appears to interact with the N-terminal portion of the receptor since deletion of these last five amino acids in the receptor results in a conformational change that shields Tyr86 from solvent. This amino acid is located within the presumed N-terminal targeting signal (NTTS) binding domain. In contrast, removal of aa30−60 exposes this aromatic amino acid partly to solvent.

In the preceding paper we show that aa48−99 is involved in recognizing NTTS and that aa30−60 is involved in anchoring the cytosolic domain of the receptor to the membrane surface (*29*). We now can distinguish between the membrane binding domain and the receptor domain since the deletion of the first 48 amino acids results in loss of binding of the receptor to the membrane surface. However, in the presence of an NTTS peptide this protein can be targeted to the membrane, suggesting that the targeting signal also binds to the membrane during recognition by the receptor complex. In addition, we are able to demonstrate by fluorescence titration that hTom20 interacts very weakly with an N-terminal targeting sequence ($K_d = 8\ \mu M$) and in the absence of the membrane surface. This value agrees with our previous finding (*29*) from direct binding studies of the GST-fused cytosolic domain and a radiolabeled NTTS-containing protein.

MATERIALS AND METHODS

Materials. The plasmid pGEX was purchased from Invitrogen. Lipid-coated beads were prepared by NIMBUS GmBH, Leipzig, Germany. The pO(1−27) peptide was synthesized as described elsewhere (*9*). The routine procedures used in this study (e.g., SDS−PAGE[1] and fluorography) are described in ref *10* and references therein.

Plasmid Construction and Expression and Purification of GST-hTom20 and Variants. All truncations and mutations

[†] This work was supported by operating grants from the Medical Research Council and the National Cancer Institute of Canada to Dr. G. C. Shore and from the Natural Sciences and Engineering Research Council to Dr. J. Turnbull. E. Schleiff is a recipient of a fellowship from the HSP/III program from the German Academic Association Service (DAAD).

* Corresponding authors. Address: 3655 Drummond 906b, Montreal, Canada H3G 1Y6. Tel: 1-514-398-8168. Fax: 1-514-398-7384. E-mail: schleiff@med.mcgill.ca and jturn@vax2.concordia.ca.

[‡] McGill University.

[§] Concordia University.

[1] Abbreviations: GST, glutathione *S*-transferase; SDS−PAGE, sodium dodecyl sulfate−polyacrylamide gel electrophoresis; pODHFR, targeting signal of preornithine carbamyl transferase fused to dihydrofolate reductase; Tom, translocase on the outer mitochondrial membrane; aa, amino acid.

S0006-2960(98)00746-6 CCC: $15.00
Published on Web 09/01/1998

of hTom20 were generated and purified as outlined in the preceding paper. The cleaved product was passed over a Mono S column (Pharmacia) and finally dialyzed against 20 mM sodium phosphate pH 7.4, 150 mM NaCl, and 1 mM dithiothreitol (DTT). Any exceptions are indicated in the text.

Circular Dichroic (CD) Spectroscopy Measurements. CD spectra were recorded in a Jasco 710 spectropolarimeter. Protein samples were placed in a thermostated 0.1 cm path length quartz cell for measurements from 184 to 260 nm and in a cell with a 1 cm path length for measurements from 250 to 320 nm. All measurements were recorded at 23 °C (except temperature-dependent measurements) with 1 nm bandwidth, 0.2 nm resolution, and multiple accumulations averaged for each sample. To monitor unfolding of the protein by guanidine−HCl or urea, the protein was incubated for 24 h at 4 °C with the denaturant prior to recording measurements. For detection of the refolding, total denatured protein was dialyzed against lower concentration denaturant for 24 h at 4 °C and the CD spectrum was recorded subsequently. For temperature denaturation experiments, spectra from 190 to 320 nm were obtained over the range 20−90 °C with incremental increases of 5 °C by manual adjustment of the circulating water bath. Samples were allowed 20 min equilibration time at the desired temperature before measurements were taken. Contributions to the signal by buffer were subtracted, and ellipticity in millidegrees was converted to mean residue ellipticity (deg cm^2 $dmol^{-1}$ $residue^{-1}$) or change in molar extinction coefficient (M^{-1} cm^{-1}). Protein concentrations were determined using Biorad reagent, and results were confirmed by amino acid analysis.

The unfolding of the backbone of the intact and truncated version of the cytosolic domain during chemical denaturing were monitored by far-UV CD spectroscopy. The unfolding appears to follow a two-state transition (discussed in Results) and hence was analyzed according to the method of Pace (*11*):

$$\mathrm{N} \leftrightarrow \mathrm{U} \tag{1}$$

where N and U represent the native and unfolded protein, respectively. The equilibrium constant between the native and unfolded state is

$$K = [\mathrm{U}]/[\mathrm{N}] \tag{2}$$

and is related to the unfolded fraction of the protein (F_u) and the standard Gibbs free energy of denaturation (ΔG_d) by

$$\Delta G_d = -RT \ln K = -RT \ln(F_u/(1 - F_u)) \tag{3}$$

where T is the absolute temperature and R is the universal gas constant. ΔG_d was plotted versus denaturant concentration, and the data were fitted by least-squares analysis to

$$\Delta G_d = \Delta G_{d,aq} - m[\text{denaturant}] \tag{4}$$

to yield a value for ΔG_d which represents the minimum value for the conformational stability of the protein in the absence of denaturant ($\Delta G_{d,aq}$) and the dependence of the transition from native to unfolded state with the amount of denaturant (m). The denaturant concentration at the half-maximal ellipticity ($D_{1/2}$) was calculated by fitting the data to a sigmoidal equation by least-squares analysis.

Fourth Derivative Spectroscopy. Absorption spectra were recorded on a Cary spectrophotometer, and data were transformed using SigmaPlot. All measurements were performed at 23 °C using a 1 cm path length quartz cuvette, a bandwidth of 1 nm, a scan rate of 0.1 nm/s, a step width of 0.1 nm, and a derivative interval of 2.6 nm. The derivative of each spectrum was calculated after correcting for the buffer signal. Spectra were fitted by least-squares analysis and by using standard curves of free phenylalanine and tyrosine in 100% water, 50% water/50% ethanol, and 100% ethanol.

Fluorescence Spectroscopy Measurements. Fluorescence spectra were recorded with a Shinadzu fluorescence spectrometer using an excitation wavelength of 274 nm for tyrosine or 295 nm for tryptophan and a bandwidth of 4 or 2 nm, respectively. All emission spectra were recorded from 295 (305 to 420 nm at 23 °C with 0.5 nm/s scan rate, 0.2 nm step width, and 2 nm bandwidth using a 1 cm path length cell. Each spectrum was baseline and instrument corrected. The quenching constant of the quenching of tyrosine 86 using increasing amounts of acrylamide was determined using the Stern−Volmer equation

$$F_o/F = 1 + K_{sv}[Q] \tag{5}$$

where F_o represents the fluorescence in the absence of quencher, F is the fluorescence in the presence of quencher (both in arbitrary units), [Q] is the concentration of the quencher (in M), and K_{sv} is the Stern−Volmer quenching constant (in M^{-1}) for collisional quenching.

Binding Measurements. The binding of the matrix targeting signal of pODHRF, pO(1−27), to Δ30hTom20$_{Tyr\rightarrow Trp86}$ was followed by incubating 20 μM Δ30hTom20$_{Tyr\rightarrow Trp86}$ in 20 mM sodium phosphate pH 7.4, 100 mM NaCl, and 1 mM DTT at 20 °C with increasing amounts of pO(1−27) peptide. The change of the tryptophan fluorescence of hTom20$_{Tyr\rightarrow Trp86}$ at 348 nm was used to determine the dissociation constant. The excitation wavelength chosen was 295 nm to avoid contribution by Tyr27 of the pO(1−27) peptide. The signal change at 360 nm yielded a higher ratio of $(F/F_o)_{max}$. $(F/F_o)_{max}$ was then used to calculate the free peptide concentration under the assumption of a 1:1 binding behavior. The dissociation constant was calculated using following equation

$$F/F_o = [\mathrm{pO}]_{free}/(K_d + [\mathrm{pO}]_{free}) \tag{6}$$

where F_o represents the fluorescence of the Trp86 in the absence of precursor peptide, F is the tryptophan fluorescence in the presence of peptide, $[\mathrm{pO}]_{free}$ represents the free peptide concentration, and K_d is the dissociation constant (in M).

Binding of the cytosolic domain of hTom20 to phosphatidylcholine/phosphatidylserine (PC/PS) (4:1)-coated beads was performed as described in the preceding paper. The 5 mM lipid equivalent was incubated with 10 μM protein for 16 h at 4 °C. Supernatant was removed, and beads were boiled in the SDS sample buffer followed by separation on SDS−PAGE and Western blot analysis.

RESULTS

Probing the Stability of the N-Terminal Domain. To determine the effect of aa30−60 on the structure of the

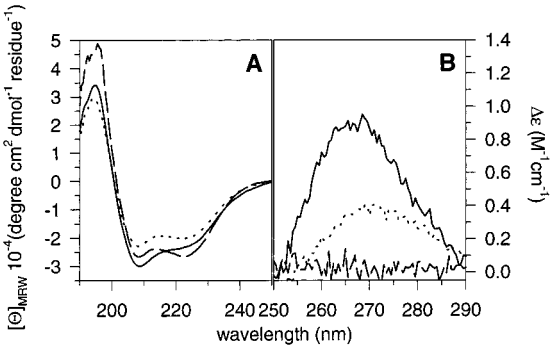

FIGURE 1: CD spectra of the native cytosolic domains of hTom20 CD spectra of native proteins Δ30hTom20 [5 mM (···)], Δ30hTom20Δ141−145 [5 mM (—)], and Δ60hTom20 [10 mM (- - -)] were recorded in the far-UV (190−250 nm) (A) and in the near-UV (250−290 nm) (B). All measurements were recorded of protein in a buffer of 20 mM sodium phosphate pH 7.4, 150 mM NaCl, and 1 mM DTT. Cuvettes with a path length of 0.1 and 1 cm were used for measurements recorded in the far-UV and near-UV, respectively. Values were buffer-subtracted, and far-UV measurements were corrected further for differences in protein concentration and primary sequence. Spectral tracings shown in A and B represent the average of 15 accumulations.

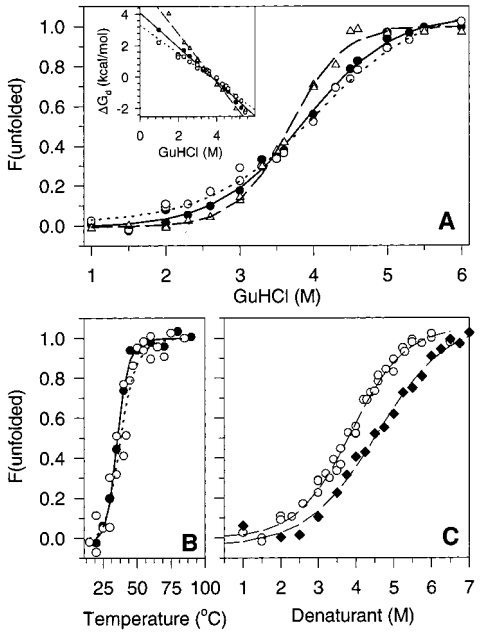

FIGURE 2: Denaturation of Δ30hTom20 by temperature, guanidine−HCl, and urea. Shown are the effects of guanidine−HCl (A) and temperature (B) on the CD of Δ30hTom20 (○- -○), Δ30hTom20Δ141−145 (●—●), and Δ60hTom20 (△- -△) using the same concentrations of protein as listed in Figure 1. Chemical denaturation of Δ30hTom20 (C) was followed using urea (◆) and guanidine−HCl (○). The molar ellipticity of the proteins at 222 nm was used to record the effects of guanidine−HCl, while the effect of temperature was monitored at 265 nm. Denaturation experiments were performed once except for the thermal unfolding of Δ30hTom20 which shows all values from two separate experiments. The measurements used to generate the curves in A, B, and C represent the average of 15 accumulations. The curves are drawn from least-squares analysis of the data fit to a sigmoidal equation. The linear dependence of the free energy of unfolding, ΔG_d, versus guanidine−HCl is shown in the inset. For experimental details, see Figure 1.

cytosolic domain of hTom20, we expressed and purified the entire cytosolic domain, Δ30hTom20 (aa30−145), and the truncated variant, Δ60hTom20 (aa60−145). Our findings in the preceding paper suggest the C-terminal region (aa141−145) may influence the conformation of the N-terminal region (aa30−60). Hence, we also constructed a protein missing the five amino acids of the C-terminal end, Δ30hTom20Δ141−145. Far- and near-UV CD spectroscopy (Figure 1A,B) were then used to determine the response of the cytosolic domain and its variants to denaturation by guanidine−HCl or temperature. Shown for each protein in Figure 2 is the loss of ellipticity of the backbone absorption at 222 nm versus guanidine−HCl (A) or the decrease in the aromatic CD at 265 nm versus temperature (B). The apparent monophasic unfolding of the backbone by guanidine−HCl (Figure 2A) and the fact that renaturation and denaturation curves are comparable (not shown) allow us to assume a two-state (all-or-none) mechanism of unfolding. From these data we calculated the thermodynamic parameters listed in Table 1. All three proteins are denatured at about the same concentration of denaturant ($D_{1/2}$ value in Table 1). However, the conformational stability of Δ60hTom20, as indicated by the free energy of unfolding in the absence of denaturant, $\Delta G_{d,aq}$, appeared almost 2 times higher than Δ30hTom20 (Figure 2A, Table 1). Careful examination of the data indicates this is because the slope of the denaturation curve (m) for Δ60hTom20 is twice that of Δ30hTom20. Moreover, the increase in the value of m represents an increase of the surface area of the protein that becomes freshly exposed to the denaturant during unfolding (*11, 12*), as would be expected for the denaturation of a more compactly folded protein. Interestingly, the $D_{1/2}$ values for all three proteins are surprisingly high (at about 4 M rather than 2−3 M as with many proteins—for example, see ref *13*), indicating that the secondary structure of the protein is quite resistant to denaturation by guanidine−HCl. Monera and co-workers (*14*) have shown that the unfolding of the protein secondary structure by guanidine−HCl will indicate stabilizing contributions by hydrophobic/nonionic interactions only. In contrast, stabilization of the secondary structure by electrostatic *and* hydrophobic/nonionic intramolecular interactions can be monitored in urea. Given that the $D_{1/2}$ values for unfolding using guanidine−HCl are surprisingly high, it was interesting to compare the denaturation using guanidine−HCl and urea (Figure 2C and Table 1). Values for $D_{1/2}$ and ΔG are in the same range for both denaturants, suggesting that hydrophobic interactions are strongly involved in stabilizing secondary structural components of the cytosolic domain.

The thermally induced loss of the protein *tertiary* structure, resulting in changes in the environment of Tyr86, can be monitored at 265 nm (Figure 2B). This probe was chosen since the CD of the full-length cytosolic domain in the near-UV (250−290 nm) shows a broad maximum band at about 270 nm (Figure 1B, dotted line). This spectrum most likely represents a predominant contribution from the single tyrosine (Tyr86) found within the cytosolic domain. The protein contains no tryptophan residues. Moreover, the $\Delta\epsilon_M$ value for this band at 270 nm is 0.4 M^{-1} cm^{-1} and within the range typically observed for tyrosines in proteins and model compounds (*15*−*17*). Surprisingly, the spectrum does not reveal the sharp but less intense fine structure between 256 and 268 nm usually associated with phenylalanine groups, of which there are four in the protein. Estimation of the midpoint of the transitions (T_m) showed that

Table 1: Effects of Guanidine−HCl, Urea, and Temperature on the Full-Length and the Truncated Cytosolic Domain of HTom20

variable parameter	(nm)	urea	guanidine−HCl		
		Δ30hTom20	Δ30hTom20	Δ30hTom20Δ141−145	Δ60hTom20
$D_{1/2}$ (M)[a]	222	4.7 ± 0.1	4.03 ± 0.07	3.88 ± 0.04	3.7 ± 0.1
m (kcal/mol/M)[b]		0.64 ± 0.09	0.82 ± 0.08	1.00 ± 0.07	1.6 ± 0.1[d]
$\Delta G_{d,aq}$ (kcal/mol)[b]		2.9 ± 0.5	3.3 ± 0.3	3.9 ± 0.2	6.0 ± 0.4[d]
T_m (°C)[a]	265	38 ± 3		35 ± 4	nd[c]

[a] Values are calculated from the inflection points of the curves in Figure 1C, D by fitting the data to a sigmoidal equation using least-squares analysis. Values represent the mean ± SE. [b] Determined by fitting the data in Figure 1C,D to the equation $\Delta G_d = \Delta G_{d,aq} - m$[denaturant] using least-squares analysis (*11*). Values represent the mean ± SE. [c] Value not determined since no CD signal observed. [d] Values are comparable to those reported for other small, globular, well-characterized proteins (*27*, *28*).

Δ30hTom20 and Δ30hTom20Δ141−145 exhibited similar thermal stabilities (Table 1) and paralleled the results found with guanidine−HCl denaturation. The low transition temperature (around 37 °C) suggests, however, that the tertiary structure of the region around Tyr86 is very flexible. To test this, we followed the kinetics of denaturation by temperature at both 222 and 265 nm (data not shown). The cytosolic domain of hTom20 was placed in a 90 °C preheated cell, and the CD spectrum was recorded every 5 min. The signal at 265 nm was decreased to the background value within 5 min, indicating that the tertiary structure is rapidly unfolded. In contrast, the secondary structure is essentially unaltered even over an extended time period (greater than 120 min). These results again highlight the resiliency of the protein's secondary structure and the flexibility of the tertiary structure of the N-terminal region containing Tyr86.

Structural Properties of the N-Terminal Targeting Signal Binding Region of hTom20. The spectral properties of Tyr86 were exploited in order to assess the tertiary structure of the NTTS binding domain of hTom20 (aa30−90). Figure 1B shows that N- and C-terminal truncations can alter the local environment surrounding aromatic groups in the cytosolic domain. Truncation of aa30−60 at the N-terminus of the cytosolic domain eliminates the signal at 270 nm (dashed line), implying the acquisition of considerable conformational freedom of the tyrosine. By contrast, removing five residues at the C-terminus (aa141−145) increases the signal (solid line) and causes an apparent blue shift by 4 nm, indicating that Tyr86 and possibly one or more phenylalanines are in a more constrained environment (*15*). The changes in the signal were not due to aggregation since neither of the truncated variants formed higher molecular weight species at the concentrations used in this study (data not shown).

The observations from near-UV CD spectroscopy are further supported by the results of the fluorescence quenching of the aromatic signal using acrylamide (Figure 3A and Table 2). Figure 3A shows the Stern−Volmer plot of fluorescence quenching of Tyr86 as found in the three different variants of the cytosolic domain (full-length, N-terminal truncated, and C-terminal truncated). We observed that the quenching of the fluorescence is only slightly increased by deletion of aa30−60 compared to the quenching found for the full-length cytosolic domain. Therefore, the solvent exposure of the tyrosine is virtually unchanged by deleting these 30 N-terminal residues. In contrast, the deletion of the last five residues (aa141−145) results in a dramatic decrease of the quenching of the tyrosine fluorescence. This finding implies that the C-terminal region influences the structural behavior of the N-terminus of the cytosolic domain.

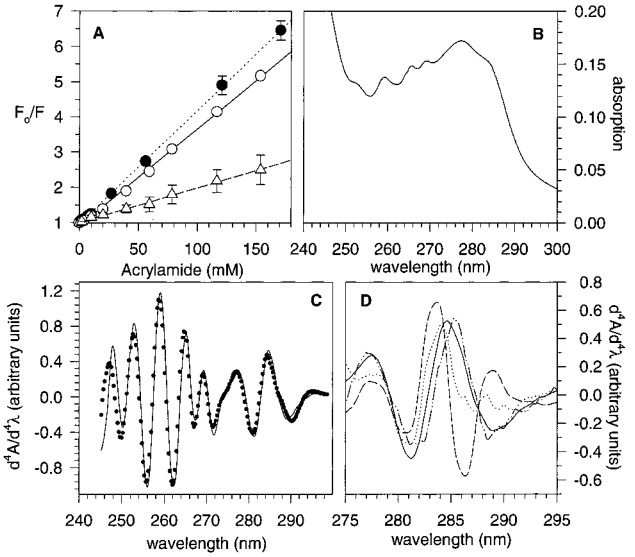

FIGURE 3: Probe of the aromatic environment using the intact and truncated variants of the cytosolic domain of hTom20. Shown in A is the quenching of the tyrosine emission at 305 nm in the presence of increasing amount of acrylamide. Open circles represent the quenching for Δ30hTom20, closed circle for Δ60hTom20, and open triangle for Δ30hTom20Δ141−145. The data were fitted to the equation for a straight line by linear regression. Shown in B is the absorption spectrum of Δ30hTom20 and in C the fourth derivative calculated from this spectrum (—). Points in C represent the least-squares fit of the fourth derivative of the spectrum in B to standard tyrosine and phenylalanine fourth derivative spectra in different environments. D shows the fourth derivative spectra of Δ30hTom20Δ141−145 (- - -), Δ60hTom20 (···), Δ30hTom20 (—), and Δ30hTom20 in 1% octylglucoside (- ·· -) as calculated from absorption spectra (not shown). Shown is the region typically observed for tyrosine absorption. Data represent the average value of at least two independent measurements.

In addition, we measured the absorption spectrum of Δ30hTom20 (Figure 4B) and calculated the fourth derivative of this spectrum (Figure 4C,D) and that of Δ30hTom20 in detergent, Δ60hTom20, and Δ30hTom20Δ141−145 (Figure 4D). The fourth derivative of the spectra was used for the following reasons: (a) the derivate can reveal the presence of constituted bands that are not apparent in the original spectra; (b) the bands are better resolved in the fourth than in the second derivate of the spectra; (c) the wavelength maxima of the fourth derivate agree more closely to the wavelength maxima of the original spectrum than to those of the second derivate (*18*). The fourth derivative spectra were then fitted with a set of spectral standards comprising free tyrosine and phenylalanine in 100% water, in 100% ethanol, and in 50% water/50% ethanol (example is shown for Δ30hTom20 in Figure 4C). This experiment yields

Table 2: Effect of Deletion in the Cytosolic Domain on the Solvent Accessibility of the Proteins around Aromatic Amino Acids[a]

protein	Phe (%$H_2O_{exposure}$)	Tyr (%$H_2O_{exposure}$)	λ_2 (nm)[a]	K_{sv} (M^{-1})
Δ30hTom20 in 1% OG	0	20	285.3	
Δ30hTom20	0	28	284.6	27 ± 1
Δ60hTom20	0	45	284.0	32 ± 1
Δ30hTom20Δ141−145	0	81	283.7	10 ± 1

[a] The percentage exposure of the proteins' tyrosine/phenylalanine residues to water was determined by a least-squares fit to the fourth derivative spectrum of the construct using standard spectra for free tyrosine and phenylalanine in 100% water, 100% ethanol, and 50% ethanol. The quenching was determined using fluorescence of the tyrosine. The quenching constant was calculated using eq 5. [b] According to ref *19*.

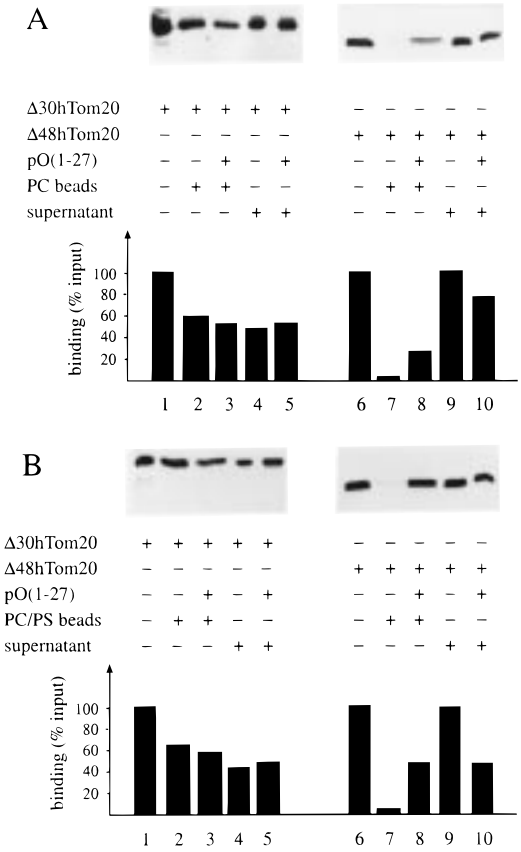

FIGURE 4: Binding of Δ48hTom20 and Δ30hTom20 to the lipid surface. The binding of the cytosolic domain of hTom20 (lanes 1−5) and its variant (lanes 6−10) to the membrane surface under various conditions were quantified by densitometry of Western blots (WB) using anti-Tom20 antibody. One WB is shown as example. The histogram represents the average of three independent measurements (SE < 10%). Lanes 1 and 6 represent the signal from Δ30hTom20 and Δ48hTom20 only. Lanes 2, 3, 7, and 8 show the result of the interaction of receptor and beads in the absence (2, 7) or the presence (3, 8) of 0.3 mM pO(1−27) peptide. Lanes 4, 5, 9, and 10 represent the amount of protein remaining in supernatant in the absence (4, 9) or presence (5, 10) of peptide.

information about the polarity of the environment of the tyrosine and phenylalanines of the protein (results are summarized in Table 2). Consistent with the result of the fluorescence quenching, the deletion of the first 30 residues (Δ60hTom20) of the cytosolic domain does *not* completely expose Tyr86 to the surface of the protein. In contrast, the least-squares fit of the fourth derivative of the absorption spectrum of the cytosolic domain containing the truncation of the last five residues (Δ30hTom20Δ141−145) to that of

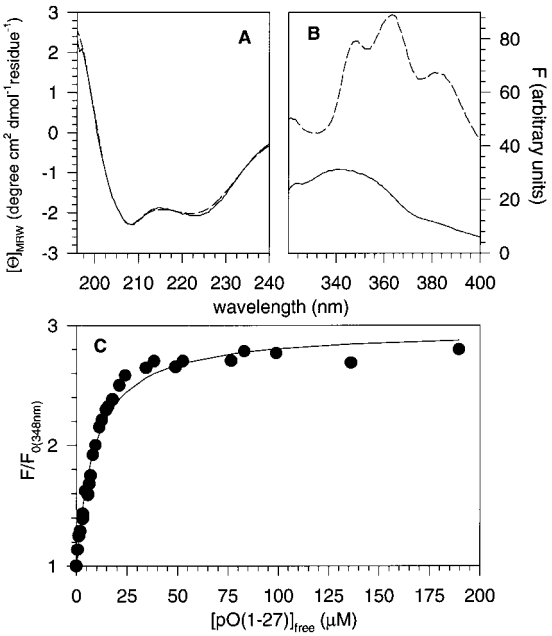

FIGURE 5: Binding of pO(1−27) peptide to $\Delta30hTom20_{Tyr\rightarrow Trp86}$. Shown in A is the CD spectra of Δ30hTom20 (- - -) and $\Delta30hTom20_{Tyr\rightarrow Trp86}$ (—). For experimental conditions see legend of Figure 1. The fluorescence spectrum of Δ30hTom20 (20 μM) in the absence (—) and presence of 150 μM pO(1−27) peptide (- - -) was measured in B. In C the binding curve for the interaction of pO(1−27) peptide and $\Delta30hTom20_{Tyr\rightarrow Trp86}$ using the change in tryptophan fluorescence intensity as the probe for the interaction is shown. The data points represent measurements at various peptide concentrations, and the line represents the best fit of one set of experimental results to eq 6. The binding was measured four times with consistent results.

the standard tyrosine and phenylalanine spectra in different environments suggests that Tyr86 becomes surface exposed (Table 2). This latter observation at first appears to contradict our previously mentioned spectroscopic results. However, Padros and co-workers (*19*) have demonstrated that a linear dependence of the dielectric constant (ϵ) with the shift of the signal in the fourth derivative spectrum is followed only in a range of $\epsilon = 20-80$ (ethanol gives a value of $\epsilon = 24.3$); tyrosine in an environment with ϵ smaller than 20 yields fourth derivative spectra that do not correlate well with ϵ of the environment. Furthermore, Simson and Perahia (*20*) have found that the value of ϵ inside proteins is about 3−5. The magnitude of the spectral shift determined for tyrosine in chloroform ($\epsilon = 4.8$) (*19*) parallels that found for the tyrosine in Δ30hTom20Δ141−145. Taken together, the results from absorption spectroscopy and the fluorescence quenching imply that Tyr86 within Δ30hTom20Δ141−145 is not surface exposed, but sits, rather, in the protein's interior.

Function of the N-Terminal Targeting Signal Binding Region of hTom20. Our most recent studies suggest that the N-terminal targeting signal binding region is located between aa48−90 of the receptor while aa30−60 are involved in binding hTom20 to the lipid surface (*29*). In this report we demonstrate that these two regions are *not* overlapping. We used beads coated with neutral (PC) (Figure 4A) and negatively charged (PC/PS) lipids (Figure 4B) to study the binding of the cytosolic domain of hTom20 to the membrane surface. Our results show that *only* Δ30hTom20 binds to the membrane surface, not Δ48hTom20

(Figure 4A, lanes 2 and 7). This interaction is independent of the surface charge of the membrane since similar results were obtained in the presence of neutral (Figure 4A) or negatively charged lipids (Figure 4B, lanes 2 and 7). In addition, Δ30hTom20 cannot be displaced from the membrane by pO(1−27), a peptide representing the matrix targeting signal sequence of pOCT (Figure 4A,B lanes 2 and 3). Both findings suggest that the membrane binding region and the NTTS recognition site (aa48−90, see preceding paper) are not overlapping. Interestingly, however, in the presence of pO (1−27) peptide, Δ48hTom20 does bind to the membrane surface (Figure 4A, lane 8), and this binding is enhanced in the presence of charged lipids (compare Figure 4A, lane 8, with Figure 5B, lane 8).

The present study represents the first cited report using spectral titration to determine the binding affinity of preproteins to mitochondrial receptor proteins. Toward this end, we replaced Tyr86 by tryptophan and used the change in tryptophan fluorescence to monitor the binding of the cytosolic domain of the receptor to the pO(1−27) peptide. As shown in Figure 5A, this mutation did not alter the secondary structure of hTom20 as detected by far-UV CD spectroscopy since the spectra of the wild-type and mutant protein are superimposable. However, during interaction of the receptor with the matrix targeting signal, the tryptophan spectrum of $Tom20_{Tyr\rightarrow Trp}$ is altered—we see an increase in the signal at 348 nm as well as at 360 nm (Figure 4B). Quantification of the difference in fluorescence intensity at either wavelength varies hyperbolically as a function of the free peptide concentration (Figure 5C), yielding a dissociation constant (K_d) of 8 ± 1 μM.

DISCUSSION

The hTom20 receptor comprises a membrane anchor domain (aa5−25) and a cytosolic domain (aa30−145). We have defined the receptor's supersecondary structure, shown in Figure 6, using conserved proline residues (and Gly89) to roughly mark the boundaries between regions of structural and/or functional significance (e.g., areas enriched in particular charges or conserved motifs). This model and can be applied generally to all forms of Tom20 even if very recent work indicates that there may be a difference in the component composition of the receptor complex between the *Saccharomyces cerevisiae*/*Neurospora crassa* and mammalian import systems (*21*, *22*), since the Tom20 receptors from rat, *N. crassa*, *S. cerevisiae*, and potato share common functional motifs and specific amino acid residues.

Our most recent studies (*29*) have shown that the aa30−90 region of hTom20 has two roles: (a) to stabilize the cytosolic domain on the membrane surface and (b) to bind NTTS-containing preproteins. However, we did not determine if these regions are overlapping. In earlier studies, it was proposed that the C-terminus (aa141−145) of the protein might also be involved in recognizing preproteins containing an NTTS (*23*). However, our previous binding studies using Δ30hTom20Δ141−145 fused to glutathione *S*-transferase and a radiolabeled preprotein containing an NTTS (*29*) did not show a direct interaction of this C-terminal region with NTTS-containing proteins. In addition, there is little known structurally about the cytosolic domain of Tom20. We believe that the cytosolic domain of the receptor, especially the N- and C-terminal regions, warrant further investigation.

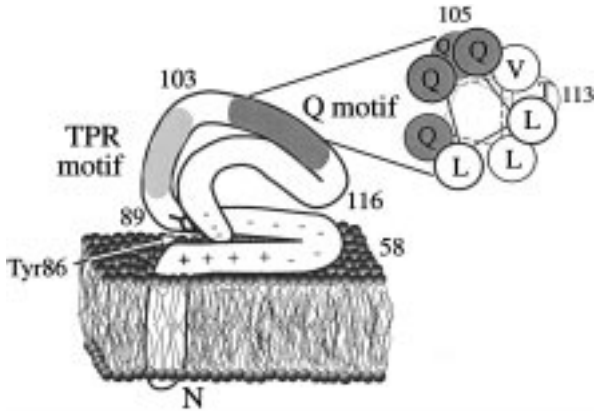

FIGURE 6: Model illustrating the mode of binding of hTom20 to preproteins. Model of a low-resolution structure of Tom20 illustrating the helical wheel projection of the binding domain of hTom20 (aa105−113) which is proposed to interact with internal signal containing proteins. See Discussion.

Our results suggest that the secondary structure of the cytosolic domain of hTom20 is stabilized by hydrophobic interactions since urea and guanidine−HCl denaturation yield similar values of $D_{1/2}$ and ΔG (*14*). This finding implies that most of the charged amino acids which are located at the N- and C-termini are not involved in intramolecular interactions but rather are crucial for the function of the protein, such as binding to preproteins, forming the receptor complex, and stabilizing the protein on the membrane surface. Our results further indicate that the secondary structure of hTom20 is very stable and shows remarkable resistance against temperature and chemical denaturation (Figure 2A,C). In contrast, however, the tertiary structure of the polypeptide surrounding Tyr86 is very flexible. The amino acids surrounding Tyr86 (QGEYEKGV) are predicted (PHD prediction program, (*24*)) to be in a loop region. The T_m value (∼35−38 °C) is of physiological relevance. A T_m value at the in vivo temperature of mammalian cells (Figure 2B and Table 1) suggests that the tertiary structure could be stabilized either by interactions with other components of the receptor complex or the membrane. Another explanation could be that this flexibility is important for preprotein recognition since the region aa50−90 surrounding the Tyr86 was found to be involved in this interaction.

Further evidence that the N-terminal region of the cytosolic domain is more loosely folded then other regions of the protein comes from our previous studies (*29*) using size exclusion chromatography and limited proteolysis. We observed that Δ60hTom20 migrates as a more globular protein than Δ30hTom20 through size exclusion gel and that Δ30hTom20 is susceptible to cleavage by limited proteolysis only in the N-terminal region (aa30−60).

The spectral studies presented in this report show that the C-terminal region (141−145) of the receptor interacts with the NTTS binding region and stabilizes the native more loosely folded structure of the cytosolic domain. This finding parallels the result observed using size exclusion chromatography (*29*) that the deletion of this region results in a "collapsed" form of the receptor migrating as a more globular protein than the entire cytosolic domain. We suggest that this occurs by the C-terminal region folding back into the protein core and stabilizing a relaxed form of the NTTS binding domain of hTom20 (see Figure 6). The C-terminus

may be involved indirectly in the binding of these preproteins by merely maintaining the structural integrity of the NTTS binding site of the receptor rather than interacting directly with NTTS-containing proteins. This may explain why an earlier study (*23*) has reported a dependence of the binding of NTTS-containing proteins on the C-terminal domain.

Despite the fact that hTom20 recognizes targeting signals with high specificity (see preceding paper and ref *10*), we detected experimentally a rather high dissociation constant for the complex with a matrix targeting signal (Figure 5) ($K_d = 8\ \mu M$) or with a preprotein ($K_d = 2.6\ \mu M$) (*29*). Since dissociation constants of protein−protein interactions are normally in the nM range (*25*), we conclude that the cytosolic domain hTom20 possesses a low affinity for preproteins in vitro. One explanation for this behavior would be that there is a conformational change of the receptor upon preprotein binding to a form with lower affinity. Such a process could accommodate the specific recognition of preproteins but guarantee the release of the preprotein from the receptor in its transport to the translocation pore. Alternatively a strong initial binding might not be needed if the preprotein will be actively transported to hTom20 and if this receptor acts only as translocator.

A question remained if the membrane and the NTTS binding domain were overlapping. The present study shows that while the cytosolic domain of hTom20 binds to the membrane, the cytosolic domain lacking aa30−48 does not (Figure 4). Therefore, the region on the receptor interacting with the membrane surface must encompass aa30−48 and is clearly distinct from the NTTS binding domain (aa48−90) (*29*). Moreover, the binding of the cytosolic domain to the membrane surface is very specific since the partition coefficient was found to be very high (for uncharged lipids $K_p = 1.3 \times 10^5\ M^{-1}$) (*29*) and cannot be disrupted even in the presence of 0.3 mM pO(1−27) peptide (Figure 4). Interestingly, however, in the presence of this peptide the truncated cytosolic domain (Δ48hTom20) can be "targeted" to the membrane (Figure 4), and this "targeting" is increased in the presence of negatively charged lipids. These observations imply that the binding of Δ48hTom20 to the surface can be mediated by the pO peptide. In further support of this idea, Skerjanc (*26*) has shown that the affinity of pO-(1−27) peptide for the membrane surface is greater for a negatively charged surface. The observation that Δ48hTom20 binds to the membrane *in the presence* of the NTTS peptide (Figure 4) and that the receptor has a higher affinity for the matrix targeting signal in an α-helical conformation induced by a hydrophobic environment (see preceding paper and ref *7*) implies that the signal is membrane-bound while recognized by hTom20.

ACKNOWLEDGMENT

We are indebted to Dr. J. Kornblatt and Dr. W. Findlay for helpful discussions during performance the fourth derivative and fluorescence spectroscopy, respectively, and in particular to Dr. G. C. Shore for support.

REFERENCES

1. Sollner, T., Griffiths, G., Pfaller, R., Pfanner, N., and Neupert, W. (1989) *Cell 59*, 1061−1070.
2. Sollner, T., Pfaller, R., Griffiths, G., Pfanner, N., and Neupert, W. (1990) *Cell 62*, 107−115.
3. Haucke, V., Lithgow, T., Rospert, S., Hahne, K., and Schatz, G. (1995) *J. Biol. Chem. 270*, 5565−5570.
4. McBride, H. M., Goping, I. S., and Shore, G. C. (1996) *J. Cell Biol. 134*, 307−313.
5. Komiya, T., Rospert, S., Schatz, G., and Mihara, K. (1997) *EMBO J. 16*, 4267−4275.
6. Bolliger, L., Junne, T., Schatz, G., and Lithgow, T. (1995) *EMBO J. 14*, 6318−6326.
7. Schleiff, E., Shore, G. C., and Goping, I. S. (1997) *J. Biol. Chem. 272*, 17784−17789.
8. Brix, J., Dietmeier, K., and Pfanner, N. (1997) *J. Biol. Chem. 272*, 20730−20735.
9. Gillespie, L. L., Argan, C., Taneja, A. T., Hodges, R. S., Freeman, K. B., and Shore, G. C. (1985) *J. Biol. Chem. 260*, 16045−16048.
10. Schleiff, E., Shore, G. C., and Goping, I. S. (1997) *FEBS Lett. 404*, 314−318.
11. Pace, C. N. (1986) *Methods Enzymol. 131*, 266−280.
12. Greene, R. J., and Pace, C. N. (1974) *J. Biol. Chem. 249*, 5388−5393.
13. Roberge, M., Shareck, F., Morosoli, R., Kluepfel, D., and Dupont, C. (1997) *Biochemistry 36*, 7769−7775.
14. Monera, O. D., Kay, C. M., and Hodges, R. S. (1994) *Protein Sci. 3*, 1984−1991.
15. Strickland, E. H. (1974) *CRC Crit. Rev. Biochem. 2*, 113−175.
16. Vuilleumier, S., Sancho, J., Loewenthal, R., and Fersht, A. R. (1993) *Biochemistry 32*, 10303−10313.
17. Findlay, W. A., Martin, S. R., Beckingham, K., and Bayley, P. M. (1995) *Biochemistry 34*, 2087−2094.
18. Butler, W. L. (1979) *Methods Enzymol. 56*, 501−515.
19. Padros, E., Morros, A., Manosa, A., and Dunach, M. (1982) *Eur. J. Biochem. 127*, 117−122.
20. Simonson, T., and Perahia, D. (1995) *Proc. Natl. Acad. Sci. U.S.A. 92*, 1082−1086.
21. Nuttall, S. D., Hanson, B. J., Mori, M., and Hoogenraad, N. J. (1997) *DNA Cell Biol. 16*, 1067−1074.
22. Armstrong, L. C., Komiya, T., Bergman, B. E., Mihara, K., and Bornstein, P. (1997) *J. Biol. Chem. 272*, 6510−6518.
23. Lithgow, T., Junne, T., Suda, K., Gratzer, S., and Schatz, G. (1994) *Proc. Natl. Acad. Sci. U.S.A. 91*, 11973−11977.
24. Rost, B., and Sander, C. (1993) *J. Mol. Biol. 232*, 584−99.
25. Schleiff, E., Schmitz, A., McIlhinney, R. A., Manenti, S., and Vergeres, G. (1996) *J. Biol. Chem. 271*, 26794−26802.
26. Skerjanc, I. S., Shore, G. C., and Silvius, J. R. (1987) *EMBO J. 6*, 3117−3123.
27. Green, S. M., Meeker, A. K., and Shortle, D. (1992) *Biochemistry 31*, 5717−5728.
28. Shirley, B. A., Stanssens, P., Hahn, U., and Pace, C. N. (1992) *Biochemistry 31*, 725−732.
29. Schleiff, E., and Turnbull, J. L. (1998) *Biochemistry 43*, 13043−13051.

BI980746Y